

Predicting broadband fan interaction noise using a random-vortex-particle method

M. Dieste, G. Gabard

ISVR, University of Southampton, Southampton, SO17 1BJ, United Kingdom

PACS: 43.28.Ra, 43.28.Lv

ABSTRACT

Broadband fan interaction noise can be simulated using synthetic turbulence as a source of sound in the linearised Euler equations solved in the time domain. In this work synthetic turbulent velocity fields are generated by a random-vortex-particle method able to generate two-dimensional isotropic turbulent flows by filtering white noise. The filter is expressed in terms of either the correlation function or the energy spectrum. Non-Gaussian spectra can also be considered such as Liepmann and von Karman energy spectra. Simulation results are presented for a two-dimensional flat plate interacting with homogeneous isotropic turbulence. The linearised Euler equations are solved with a multiblock finite-difference code where particles are launched upstream of the airfoil and convected with the mean flow following a purely Lagrangian approach. Temporal correlation is included in the random-vortex-particle method using first and second-order Langevin models. Far-field results are compared against the analytical solution derived by Amiet for airfoils interacting with homogeneous isotropic frozen turbulence. It is shown that the standard Langevin equation can lead to spurious noise sources and that a second-order model is able to provide accurate predictions.

INTRODUCTION

Due to increasingly higher bypass-ratio aircraft engines, and the associated reduction in jet noise, fan noise has become a major source of noise on modern aircrafts. Whilst tonal noise can be reduced relatively efficiently by tuning the properties of the acoustic liners, broadband fan noise remains more difficult to predict and to reduce due to its stochastic nature and wide frequency content.

Due to the large range of spatial and time scales present in turbulent flows, Direct Numerical Simulation (DNS) or Large Eddy Simulation (LES) are still too expensive to be used regularly to predict broadband fan noise in an industrial context. An alternative approach is to split the problem between the source mechanisms and the propagation of sound. The latter is solved using for instance Lighthill's analogy or the linearized Euler equations. Although this approach is cheaper than complete fluid dynamics simulations, the calculations in the source region using standard CFD techniques still remain expensive for industrial applications.

Stochastic computational methods provide a way to synthesise random turbulent fields that are not exact solutions of the fluid dynamics but that capture the key features of the turbulent sound sources, such as the energy spectrum and the length and time scales. The resulting synthetic fields is then combined with an aero-acoustic propagation model. This approach can result in accurate predictions of the generation and propagation of aerodynamic sound [5]. Originally, stochastic methods to generate turbulent flows were used mainly to simulate scalar dissipation and to obtain inflow turbulence for DNS and LES. Early attempts relied on a finite sum of Fourier modes whose parameters such as amplitudes, wavenumbers and phases are chosen randomly following certain distributions [13]. In aero-

acoustics this lead to the SNGR method [4; 3; 5]. It was found however that Fourier mode models have difficulties representing inhomogeneous turbulence [15].

Stochastic methods generating synthetic turbulence by filtering random data have also been developed [6; 12; 10]. The filter is chosen so that the statistical properties of the synthetic velocity field matches the statistical properties of the turbulent flow. A significant effort to develop filter-based methods for computational aero-acoustic is due to Ewert and co-workers [9; 11].

In the present work, a filter-based stochastic method is used to generate synthetic two-dimensional, homogeneous, isotropic turbulent flows. It requires as input several statistical properties of the turbulent flow including the energy spectrum, correlation, integral length scale or kinetic energy. We will focus on the description of the time correlation in the numerical model. A common way to model the time-dependence present in turbulent flows is to use a Langevin equation [16]. However, it will be shown here that the standard Langevin model is not well suited when coupled with a finite-difference solver for the linearised Euler equations. A second-order Langevin model is proposed to remedy the issues observed with the standard Langevin equation. The target application is the prediction of broadband fan noise and results will be presented for the case of a two-dimensional flat plate interacting with homogeneous isotropic turbulence.

In the next section the random-vortex-particle method used in this work is introduced and we discuss the use of two Langevin models to generate evolving synthetic turbulence with prescribed time correlations. Then, numerical results are presented for a flat plate in a uniform turbulent flow and compared against analytical results.

RANDOM-VORTEX-PARTICLE METHOD

The random-vortex-particle method used in this work is a filter-based model that builds upon the work of Careta *et al.* [6] and Ewert *et al.* [9; 11]. One of the distinctive features of the present model is to use a fully Lagrangian formulation for the discretisation which leads to a meshfree vortex-particle method.

Description of the model

Assuming a two-dimensional incompressible flow, the turbulent velocity field \mathbf{u}' can be expressed in terms of the stream function $\eta' = (\partial\eta/\partial y, -\partial\eta/\partial x)^T$. Following Ewert's *et al.* [11] approach, a two-dimensional turbulent flow is generated by defining η as a filtered random field

$$\eta(\mathbf{r}, t) = \int G(\mathbf{r} - \mathbf{r}', t) U(\mathbf{r}', t) d\mathbf{r}', \quad (1)$$

where the filter G controls the spatial statistics of the synthetic turbulence while the random field U controls the temporal properties of the flow. Assuming isotropic turbulence, the statistics of the turbulent velocity field and those of the stream function can be related so as to define η in terms of known parameters of the turbulent flow. An appropriate expression for the filter, G , is obtained through its relation with the correlation tensor of the flow, R_{ij} , or with the energy spectrum function, $E(\kappa)$:

$$G(r) = \frac{1}{\sqrt{2\pi}} \int_0^\infty \hat{R}(\kappa)^{1/2} J_0(\kappa r) d\kappa, \quad (2)$$

$$G(r) = \frac{1}{\sqrt{\pi}} \int_0^\infty \left(\frac{E(\kappa)}{\kappa} \right)^{1/2} J_0(\kappa r) d\kappa, \quad (3)$$

where κ is the wavenumber corresponding to the wavevector $\mathbf{\kappa}$, \hat{R} stands for the Fourier transform of R , J_0 is the Bessel function of zeroth order and $R(r) = R_{ii}(r)/2$. The stochastic field U is a zero-mean white noise with $\langle U(\mathbf{r}_1, t) U(\mathbf{r}_2, t) \rangle = \delta(\mathbf{r}_2 - \mathbf{r}_1)$.

For small spatial and temporal separations U satisfies the following properties:

$$\langle U(\mathbf{r}, t) \rangle = 0, \quad \langle U(\mathbf{r}_1, t_1) U(\mathbf{r}_2, t_2) \rangle = \delta(\mathbf{r} - t\mathbf{u}_c) R_U(t), \quad (4)$$

where \mathbf{u}_c is the convection velocity along the stream lines and $R_U(t) = \langle U(\mathbf{r}, t_1) U(\mathbf{r}, t_2) \rangle$ is the time correlation of U .

If the turbulence is assumed to be frozen then the stochastic field U seen in a frame of reference moving at the convection velocity is independent of time. Therefore

$$\frac{D_0}{Dt} U = 0, \quad (5)$$

where $D_0/Dt = \partial/\partial t + \mathbf{u}_c \cdot \nabla$ with \mathbf{u}_c the convection velocity. Hence, the time correlation of U is constant, $R_U(t) = 1$. Note that in this case only convection effects are represented by the model.

To summarise, the synthetic velocity field \mathbf{u}' can be defined in terms of a prescribed energy spectrum or a prescribed correlation function by

$$u'_x(\mathbf{r}, t) = \frac{\partial}{\partial y} \int_{\mathbb{R}^2} G(|\mathbf{r} - \mathbf{r}'|) U(\mathbf{r}', t) d\mathbf{r}', \quad (6)$$

$$u'_y(\mathbf{r}, t) = -\frac{\partial}{\partial x} \int_{\mathbb{R}^2} G(|\mathbf{r} - \mathbf{r}'|) U(\mathbf{r}', t) d\mathbf{r}', \quad (7)$$

where G satisfies either of the expressions (2) or (3) and U is a zero-mean stochastic field satisfying Eq. (4).

The velocity field of an incompressible and isotropic turbulent flow is therefore given by the random-vortex-particle method when the correlation tensor or the energy spectrum of the flow are provided. For each choice of these functions a different filter will be obtained. We begin by discussing the advantages and disadvantages of selecting different energy spectra in a two-dimensional turbulent flow. Then we will describe how the stochastic field U can be generated to account for the temporal properties of turbulent flows.

Application to different energy spectra

So far, most models using filtered random data have been based on Gaussian filters yielding Gaussian correlation and Gaussian spectra. The use of Gaussian filters do not however restrict completely the synthetic velocity field to have Gaussian energy spectra. As shown by Siefert *et al.* [17] by superimposing a collection of Gaussian filters with different length scales non-Gaussian energy spectra can be recovered. Note that this procedure implies a higher computational cost when reproducing non-Gaussian spectra instead of Gaussian spectra since a much larger number of vortices are required.

In the context of broadband fan noise Liepmann and von Karman turbulence spectra are more common [2]. And in this work a different approach from that of Siefert *et al.* is considered whereby non-Gaussian filters are directly used.

The Gaussian shape spectrum proposed by Kraichnan [13], Liepmann and von Karman spectra are respectively given by

$$E_g(\kappa) = \frac{2}{\pi^2} K \lambda^4 \kappa^3 \exp\left(-\frac{\lambda^2 \kappa^2}{\pi}\right), \quad (8)$$

$$E_l(\kappa) = \frac{16}{3\pi} K \lambda^5 \frac{\kappa^4}{(1 + \lambda^2 \kappa^2)^3}, \quad (9)$$

$$E_k(\kappa) = \frac{110}{27\pi} K \lambda \zeta^4 \frac{\kappa^4}{(1 + \zeta^2 \kappa^2)^{17/6}}. \quad (10)$$

K is the kinetic energy, λ the integral length scale of the turbulence and $\zeta = \frac{\Gamma(1/3)}{\sqrt{\pi}\Gamma(5/6)} \lambda$ where Γ stands for the Gamma function.

Analytical expressions of the filters corresponding to each of the three spectra under investigation are found by substituting the expressions above for the energy spectra in the right-hand side equation of Eq. (3).

Temporal properties of the synthetic turbulence

The effects of time correlation are included in the random-vortex-particle method (6)–(7) through first and second-order Langevin models. First-order Langevin models are commonly used to represent Brownian motions and also turbulent dissipation at large Reynolds numbers. It will be shown here that, due to numerical problems, a standard Langevin equation is not well suited as a source to the linearised Euler equations. As proposed in [17] a second-order Langevin model is considered to overcome the numerical issues observed with the Langevin equation. But note that we use here a different second-order model than that used proposed in [17].

Langevin equation

The temporal properties of the turbulence can be included in the method to generate synthetic turbulent (6)–(7) by defining the time evolution of the stochastic field U through a Langevin

equation of the form

$$\frac{D_0}{Dt}U = -\alpha U + \beta \zeta, \quad (11)$$

with initial condition $U(0) = U_0$ where U_0 is a random variable. ζ is a zero-mean white noise source such that

$$\langle \zeta(\mathbf{r}_1, t_1) \zeta(\mathbf{r}_2, t_2) \rangle = \delta(\mathbf{r}_1 - \mathbf{r}_2) \delta(t_1 - t_2), \quad (12)$$

The coefficients α and β of the Langevin equation can be related to the statistical properties of the turbulence.

The rate of change over time of the vortex-particles along the streamlines defined by the convection velocity \mathbf{u}_c can be derived from the Lagrangian version of Eq. (11):

$$\frac{\partial}{\partial t}U(\mathbf{r}'(\mathbf{r}_0, t)) = -\alpha U(\mathbf{r}'(\mathbf{r}_0, t)) + \beta \zeta(\mathbf{r}'(\mathbf{r}_0, t)). \quad (13)$$

The material derivative in the base flow, D_0/Dt , is the derivative taken along a path moving with the base flow, hence in a Lagrangian formulation it simply becomes the derivative with respect to time.

In order to ensure that the random process U is statistically stationary, its energy $\langle U(t)^2 \rangle$ must remain constant in time. This condition yields a unique definition for $\beta = \sqrt{2\alpha \langle U_0^2 \rangle}$.

A second constraint to be imposed on the stochastic field is concerned with the time correlation of U . Experimental results support an exponential time correlation of the velocity field of turbulent flows behaving as $\exp(-t/\tau)$ where τ is the integral time scale of the flow [18]. It is therefore sensible to define the stochastic field U so that its correlation in time also decays as $\exp(-t/\tau)$. This condition yields $\alpha = 1/\tau$.

Therefore, the effects of evolving turbulence can be modelled by a Langevin equation if defining the rate of change of U in time as

$$\frac{D_0}{Dt}U = -\frac{1}{\tau}U + \sqrt{\frac{2}{\tau} \langle U_0^2 \rangle} \zeta. \quad (14)$$

In order to ensure that there is a unique solution, an initial condition for U must be provided. U_0 is a random variable following a zero-mean Gaussian distribution with unit standard deviation.

The stochastic field U defined through the Langevin equation Eq. (14) satisfies the properties in Eq. (4):

$$\langle U(\mathbf{r}_1, t_1) U(\mathbf{r}_2, t_2) \rangle = \langle U_0^2 \rangle \delta(\mathbf{r} - t\mathbf{u}_c) \exp(-t/\tau), \quad (15)$$

where $\mathbf{r} = \mathbf{r}_2 - \mathbf{r}_1$. Note that in this case $R_U(t) = \langle U_0^2 \rangle \exp(-t/\tau)$. When assuming frozen turbulence, the time correlation tends to infinity, $\tau \rightarrow \infty$, and hence the right-hand side of Eq. (14) vanishes meaning that the model is only representing convection effects, $D_0U/Dt = 0$.

The source term ζ in the Langevin equation Eq. (14) is a white noise field independent of U_0 . Due to the rapidly fluctuating behaviour of ζ , the resulting stochastic field U is continuous but not differentiable in time. This lack of differentiability is thought to introduce spurious sources of noise. To overcome this problem the Langevin equation Eq. (14) is generalised so that the source term is continuous and in consequence the resulting stochastic field U is a smoother function in time.

Second-order Langevin model

In this work the approach proposed by Krasnoff *et al.* [14] is followed to formulate a second-order Langevin model that produces stationary isotropic turbulence with time correlation decaying as $\exp(-t/\tau)$. In contrast, with the second-order Langevin model proposed by Ewert *et al.* [17] only the stochastic source term is modified with respect to the Langevin equation in Eq. (14).

The generalised Langevin equation is given by:

$$\frac{D_0}{Dt}U = -\frac{1}{\tau}U + W, \quad (16)$$

with initial condition $U(0) = U_0$ where U_0 is a random variable. In contrast with the noise source ζ in the Langevin equation Eq. (14), the forcing term W is now assumed to be continuous (so it is not pure white noise) and it is also assumed to be correlated with U .

The rate of change over time of the random field U along the streamlines defined by the convection velocity, \mathbf{u}_c , can be derived from the Lagrangian version of Eq. (16):

$$\frac{\partial}{\partial t}U(\mathbf{r}'(\mathbf{r}_0, t)) = -\frac{1}{\tau}U(\mathbf{r}'(\mathbf{r}_0, t)) + W(\mathbf{r}_0, t). \quad (17)$$

It can be shown that to ensure the random process U is stationary one has to use

$$R_W(t) = \langle W(t_1) W(t_2) \rangle = \langle W_0^2 \rangle \exp(-\gamma t), \quad (18)$$

with $\langle W_0^2 \rangle = \langle U_0^2 \rangle / (\tau \tau_d)$ and $\gamma = (1/\tau_d - 1/\tau)$ where we have introduced an additional time scale τ_d such that $\tau_d \ll \tau$, see Ref. [14].

The resulting time correlation is

$$R_U(t) = \exp(-t/\tau) \frac{\langle U_0^2 \rangle}{\tau - 2\tau_d} \left\{ \tau - \tau_d - \tau_d \exp\left[\left(\frac{2}{\tau} - \frac{1}{\tau_d}\right)t\right] \right\}. \quad (19)$$

It converges to $\langle U_0^2 \rangle \exp(-t/\tau)$ as $\tau_d \rightarrow 0$ satisfying the properties in Eq. (15). The influence of the additional parameter τ_d will be described later.

The stochastic source W in the Langevin equation Eq. (16) can be generated using an auxiliary Langevin equation:

$$\frac{D_0}{Dt}W = -\alpha'W + \beta' \zeta, \quad (20)$$

where ζ is a white noise source verifying

$$\langle \zeta(\mathbf{r}, t) \rangle = 0, \quad \langle \zeta(\mathbf{r}_1, t_1) \zeta(\mathbf{r}_2, t_2) \rangle = \delta(\mathbf{r}_1 - \mathbf{r}_2) \delta(t_1 - t_2). \quad (21)$$

Following the same analysis as for the Langevin equation Eq. (11), the random source W is statistically stationary with time correlation $R_W(t) = \langle W_0^2 \rangle \exp(-\gamma t)$ if one defines $\beta' = \sqrt{2\alpha' \langle W_0^2 \rangle}$ and $\alpha' = \gamma$. The initial condition $W(0) = W_0$ is a random variable following a zero-mean Gaussian distribution with variance $\langle W_0^2 \rangle = \langle U_0^2 \rangle / (\tau \tau_d)$. W_0 and U_0 are correlated verifying $\langle U_0 W_0 \rangle = \langle U_0^2 \rangle / (\tau \langle W_0^2 \rangle)$. These constraints can be met by defining W_0 such that:

$$W_0 = \frac{1}{\tau}U_0 + \sqrt{\frac{\gamma}{\tau}} \xi, \quad (22)$$

where ξ is an independent zero-mean random variable with unit variance. Note that Eq. (22) verifies $W_0 = 0$ for the case of frozen turbulence ($\tau, \tau_d \rightarrow \infty$).

To summarise, the combination of Eq. (16) and Eq. (20) forms a second-order Langevin model given by:

$$\begin{cases} \frac{D_0}{Dt} U = -\frac{1}{\tau} U + W, \\ \frac{D_0}{Dt} W = -\gamma W + \sqrt{2\gamma \langle W_0^2 \rangle} \zeta, \end{cases} \quad (23)$$

with $\gamma = 1/\tau_d - 1/\tau$. ζ is a stochastic field following a Gaussian distribution with zero mean and unit standard deviation independent from W and U . The forcing term W is now a continuous function in time which yields a smoother stochastic field U than that obtained with the Langevin equation in Eq. (14)

For the case of frozen turbulence, both time scales τ and τ_d tend to infinity. Hence the right-hand sides in the system Eq. (23) are equal to zero and the model is only representing convection effects, $D_0 U/Dt = 0$ and $D_0 W/Dt = 0$.

Numerical implementation

Discretisation

The random-vortex-particle method introduced in (6)–(7) is discretised in a fully Lagrangian approach. The following notation is introduced in order to rewrite (6)–(7) in a Lagrangian formulation. Each fluid element in the region \mathbb{S}_0 at an initial time t_0 follows a trajectory given by $\mathbf{r}'(\mathbf{r}_0, t)$, where $\mathbf{r}_0(\mathbf{r}', t)$ is its starting point and $J = |\mathbf{dr}'/\mathbf{dr}_0|$ is the corresponding Jacobian. The fluctuating component of the turbulent velocity field for a fix frame of reference (6)–(7) can be rewritten in a Lagrangian formulation yielding

$$\mathbf{u}'(\mathbf{r}, t) = \int_{\mathbb{S}_0} \mathbf{G}(|\mathbf{r} - \mathbf{r}'(\mathbf{r}_0, t)|, \lambda(\mathbf{r}')) U(\mathbf{r}_0, t) J d\mathbf{r}_0, \quad (24)$$

where $\mathbf{G} = \nabla \times (0, 0, G)$. Note that here we are making explicit the dependence of the filter on the integral length scale of the fluid, λ .

By splitting \mathbb{S}_0 into the partition $\{\mathbb{S}_{0n}\}_{n=1}^N$, Eq. (24) can be discretised

$$\mathbf{u}'(\mathbf{r}, t) = \sum_{n=1}^N \int_{\mathbb{S}_{0n}} \mathbf{G}(|\mathbf{r} - \mathbf{r}'(\mathbf{r}_0, t)|, \lambda(\mathbf{r}'(\mathbf{r}_0, t))) U(\mathbf{r}_0, t) J d\mathbf{r}_0. \quad (25)$$

Each element \mathbb{S}_{0n} can be understood as a small fluid element whose trajectory is given by $\mathbf{r}'(\mathbf{r}_0, t)$.

If the fluid elements \mathbb{S}_{0n} are small compared to the the integral length scale $\lambda(\mathbf{r}_n)$, it is possible to consider that \mathbf{G} is almost constant over each \mathbb{S}_{0n} , yielding the following approximation

$$\mathbf{u}'(\mathbf{r}, t) = \sum_{n=1}^N \mathbf{G}(|\mathbf{r} - \mathbf{r}_n(t)|, \lambda(\mathbf{r}_n)) \int_{\mathbb{S}_{0n}} U(\mathbf{r}_0, t) J d\mathbf{r}_0, \quad (26)$$

where \mathbf{r}_n is the position of \mathbb{S}_{0n} as it moves across the domain. \mathbf{r}_n can be defined as the barycenter of \mathbb{S}_{0n}

$$\mathbf{r}_n = \int_{\mathbb{S}_{0n}} \mathbf{r}'(\mathbf{r}_0, t) d\mathbf{r}_0. \quad (27)$$

Finally, Eq. (26) can be rewritten as

$$\mathbf{u}'(\mathbf{r}, t) = \sum_{n=1}^N \mathbf{G}(|\mathbf{r} - \mathbf{r}_n(t)|, \lambda(\mathbf{r}_n)) U_n(t), \quad (28)$$

by defining U_n as the weighted average of U over the n^{th} fluid element \mathbb{S}_{0n}

$$U_n(t) = \int_{\mathbb{S}_{0n}} U(\mathbf{r}_0, t) J d\mathbf{r}_0. \quad (29)$$

Therefore, the synthetic turbulent velocity field at \mathbf{r} can be interpreted as the sum of N vortices such that the n^{th} vortex is located at \mathbf{r}_n , the velocity distribution depends on the distance between the vortex and the observer and has strength U_n .

Strength of the vortex-particles

Three different methods to model the time correlation of the synthetic turbulence were described. For the case of frozen turbulence, $U(\mathbf{r}_0, t)$ is constant with respect to time yielding a constant strength of the vortices in time, see Eq. (5). Therefore, from Eq. (29), the strength of each vortex-particle, U_n , can be picked from a zero-mean random Gaussian distribution with variance

$$\int_{\mathbb{S}_{0n}} J^2 d\mathbf{r}_0. \quad (30)$$

Note that for incompressible flows $J = 1$ and U_n has unit variance. Note also that by frozen turbulence we are not just stating that the statistics of the turbulence are frozen, but also the turbulent velocity field is frozen with respect to an observer moving with the base flow.

If the loss of correlation in time is included in the model to generate synthetic turbulence by the Langevin equation in Eq. (14), then the stochastic field $U(\mathbf{r}_0, t)$ is time dependent. Integrating Eq. (13) over the fluid element \mathbb{S}_{0n} , we get that the rate of change in time of each vortex-particle is given by

$$\frac{\partial}{\partial t} U_n = -\frac{1}{\tau} U_n + \sqrt{\frac{2}{\tau}} \zeta_n(t), \quad (31)$$

where ζ_n is the random source averaged over the fluid element \mathbb{S}_{0n} :

$$\zeta_n(t) = \int_{\mathbb{S}_{0n}} \zeta(\mathbf{r}'(\mathbf{r}_0, t)) J d\mathbf{r}_0.$$

Equation Eq. (31) can be discretised using:

$$U_n(t+1) = \left(1 - \frac{\Delta t}{\tau}\right) U_n(t) + \sqrt{\frac{2\Delta t}{\tau}} \zeta_n(t), \quad (32)$$

where ζ_n is the weighted average over the fluid element \mathbb{S}_{0n} of the discrete random source ζ with zero mean and unit variance (for incompressible flows). Note that in order to accurately discretise a Langevin equation a Wiener process as source term, an increment of magnitude Δt requires an increment of magnitude $\sqrt{\Delta t}$ for the source term [7].

In this work, a second-order Langevin model is also proposed to describe the time dependence of the strength of the vortex-particles. Following the same scheme as for the Langevin equation, the second-order Langevin model Eq. (23) can be discretised in a Lagrangian formulation yielding

$$\begin{cases} U_n(t+1) = \left(1 - \frac{\Delta t}{\tau}\right) U_n(t) + \Delta t W_n(t), \\ W_n(t+1) = (1 - \gamma \Delta t) W_n + \sqrt{2\gamma \Delta t \langle W_0^2 \rangle} \zeta_n(t), \end{cases} \quad (33)$$

where W_n and ζ_n are respectively the weighted average of W and ζ over the fluid element \mathbb{S}_{0n}

$$W_n(t) = \int_{\mathbb{S}_{0n}} W(\mathbf{r}'(\mathbf{r}_0, t)) J d\mathbf{r}_0,$$

$$\zeta_n(t) = \int_{\mathbb{S}_{0n}} \zeta(\mathbf{r}'(\mathbf{r}_0, t)) J d\mathbf{r}_0.$$

Note that the rate of change of W is defined through a Langevin equation and therefore the analysis performed for deriving Eq. (32) applies.

Initial conditions for U_n and W_n and values for ζ_n at each time step must be provided. Since U_0 and ζ are random variables following a zero-mean Gaussian distribution with unit standard deviation, by definition $U_n(0)$ and $\zeta_n(t)$ follow a zero-mean Gaussian distribution with variance:

$$\int_{S_{0n}} J^2 d\mathbf{r}_0.$$

W_0 is a random variable following a zero-mean Gaussian distribution with variance $\langle W_0^2 \rangle = \langle U_0^2 \rangle / (\tau \tau_d)$.

BROADBAND FAN INTERACTION NOISE

We investigate broadband fan interaction noise in two dimensions by combining the random-vortex-particle method with the linearised Euler equations solved in the time domain. As a benchmark problem, broadband noise generated by interaction between isotropic homogeneous turbulence and a flat plate is investigated.

Linearised Euler equation solver

The aero-acoustic sound propagation model consists of an in-house parallel, multiblock finite-difference code in the time domain solving the linearized Euler equations. It uses seven-point dispersion relation preserving schemes, with an optimised six-stage Runge-Kutta method for time integration. Non-reflecting boundary conditions are imposed on the boundaries of the simulation domain. Also implemented is a selective filter that removes short wavelength components that are not well resolved. Far-field results are obtained using the Ffowcs-Williams Hawkins equation using a fixed control surface surrounding the source region.

Vortex-particles are launched upstream with a random strength and convected downstream with the mean flow. The turbulent velocity field is computed at each point of the airfoil using Eq. (28) and implemented as a slip condition in the hard wall boundary condition.

Problem definition

The test case considered is that of a flat plate with zero angle of attack interacting with homogeneous isotropic turbulence. The problem is made non-dimensional using the half-chord b , mean density ρ_0 and sound speed c_0 . The parameters are taken to be similar to the test case previously selected by Amiet [1] to validate the analytical solution against experiments. The turbulence is convected by a uniform mean flow with Mach number 0.362 and characterised by an integral length scale $\lambda = 0.07$. The kinetic energy, K , is normalised to unity.

In order to introduce the effects of the temporal correlation in (6)–(7), the Lagrangian time scale of the turbulence, τ , is required. τ is a function of the dissipation rate, ε , and a weak function of the Reynolds number. Its value can be estimated by the scaling procedure:

$$\tau \approx \frac{2K}{C_0 \varepsilon}, \quad (34)$$

where ε is the dissipation rate and C_0 an empirical constant whose value is not yet exactly defined. In this work we use $C_0 = 2.1$ as proposed by Pope in [16].

The computational domain is given by $[-1.5, 1.5] \times [-1, 1]$ with the airfoil at $[-0.5, 0.5] \times \{0\}$. The domain is divided into 6 blocks, each of them discretised by a Cartesian grid with 200 points in each direction. The time step is such that the CFL number is 0.8.

Results for frozen turbulence

In this section the generation of broadband noise due to the interaction of frozen turbulence with a flat plate is investigated.

Numerical results presented in this section for the far-field sound pressure levels (SPL) are validated against a modified version of the analytical solution proposed by Amiet [1] that accounts for a fully two-dimensional acoustic far-field. The derivation of the analytical solution can be found in [8].

The quality of the synthetic turbulence has been assessed by evaluating two-point correlations and one-dimensional spectra generated by the random-vortex-particle method along the airfoil. An extensive parametric study has been performed for Gaussian, Liepmann and von Karman filters in order to improve the accuracy of the results.

Figs. (1-3) depict the two-point correlations computed with respect to the centre of the flat plate and one-dimensional spectra in the streamwise direction and in the normal direction for the Gaussian, Liepmann and von Karman spectra respectively. The statistical behaviour of the synthetic turbulence is in very good agreement with analytical results for the three spectra. Note that the shape of the correlation is determined by the filter. Therefore, while the Gaussian spectrum yields correlations with a smooth behaviour at small distances, a much sharper slope is found for Liepmann and von Karman spectra. In addition, note also that as the one-dimensional energy spectra for the Gaussian case decays faster as the frequency increases than the one-dimensional energy spectra corresponding to Liepmann and von Karman filters.

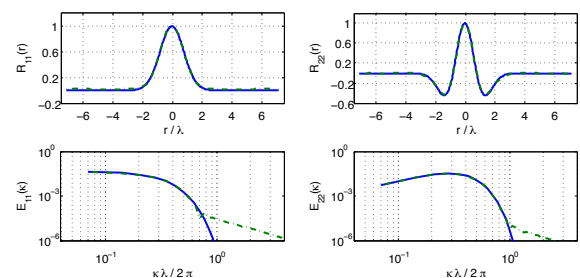


Figure 1: Analytical solution (—) against numerical results (---) obtained for Gaussian spectrum. Figures at the top correspond with correlations R_{11} and R_{22} computed with respect to the central point of the airfoil. Figures at the bottom correspond to the one-dimensional energy spectra E_{11} and E_{22} .

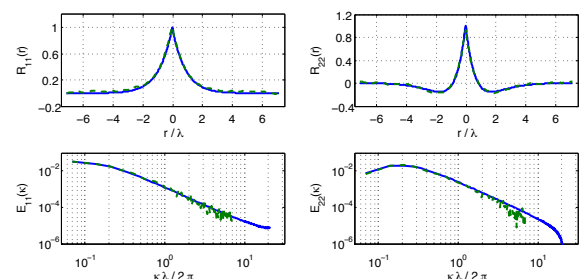


Figure 2: Analytical solution (—) against numerical results (---) obtained for Liepmann spectrum. Figures at the top correspond with correlations R_{11} and R_{22} computed with respect to the central point of the airfoil. Figures at the bottom correspond to the one-dimensional energy spectra E_{11} and E_{22} .

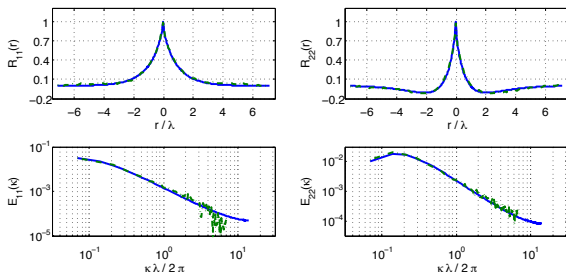


Figure 3: Analytical solution (—) against numerical results (---) obtained for von Karman spectrum. Figures at the top correspond with correlations R_{11} and R_{22} computed with respect to the central point of the airfoil. Figures at the bottom correspond to the one-dimensional energy spectra E_{11} and E_{22} .

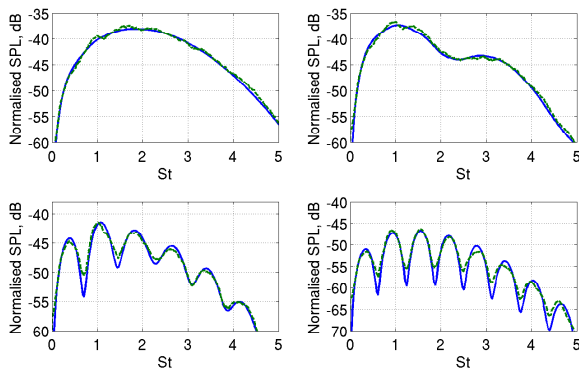


Figure 4: Normalised analytical (—) versus numerical (---) SPLs for the Gaussian spectrum and an observer located at 30° (top left), 60° (top right), 120° (bottom left), 150° (bottom right) of the airfoil.

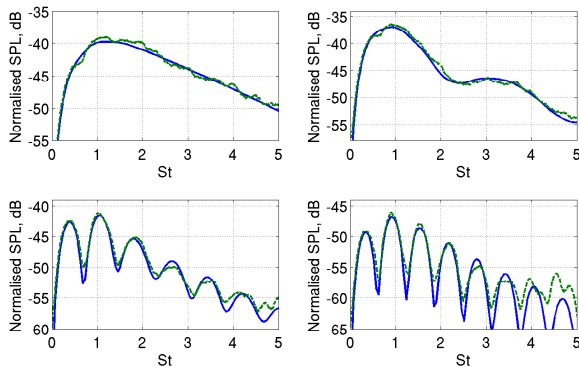


Figure 5: Normalised analytical (—) versus numerical (---) SPLs for Liepmann spectrum and an observer located at 30° (top left), 60° (top right), 120° (bottom left), 150° (bottom right) of the airfoil.

Fig. (7) shows a snapshot of the acoustic pressure field around the airfoil for the Gaussian spectrum. It shows that most of the noise is radiated from the leading edge and there is a secondary acoustic scattering at the trailing edge. This also applies with Lipemann and von Karman spectra.

The numerical power spectral density (PSD) in the far field obtained from Gaussian, Liepmann and von Karman spectra has been compared against Amiet’s solution for a fully two-dimensional problem in terms of the frequency spectrum and

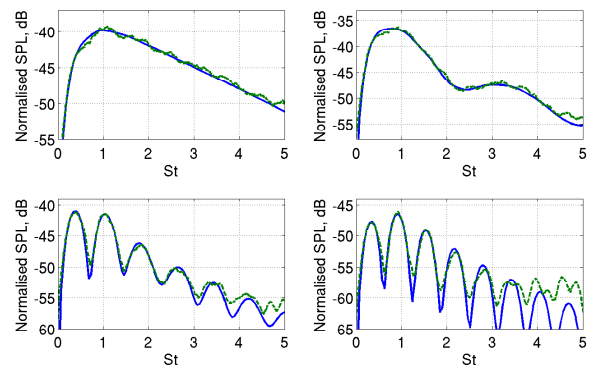


Figure 6: Normalised analytical (—) versus numerical (---) SPLs for von Karman spectrum and an observer located at 30° (top left), 60° (top right), 120° (bottom left), 150° (bottom right) of the airfoil.

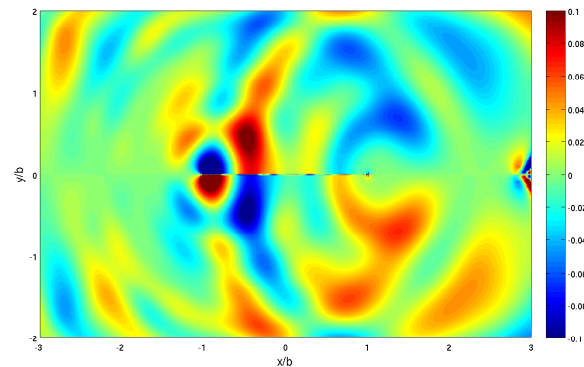


Figure 7: Snapshot of the acoustic pressure field for the Gaussian spectrum.

directivity. The PSD has been computed on a circular arc centred on the airfoil where angles are measured from the trailing edge. Sound pressure levels (SPL) in the far field presented in this work are normalised by the distance between the observer and the flat plate.

Fig. (4) shows the normalised sound pressure levels for Gaussian turbulence compared against analytical results for observers located at 30, 60, 120, 150 degrees from the downstream direction. Figs. (5, 6) depict the SPL at same locations but computed using synthetic turbulent velocity field generated with the Liepmann and von Karman spectra respectively. Noise levels are in good agreement with the analytical solution for the three spectra at all the locations. The margin of error slightly increases towards upstream directions (in particular for the von Karman spectrum) having problems to capture the oscillatory behaviour of the SPL for different Strouhal numbers.

Directivities for $St = 2.03$ and $St = 4.06$ are shown in Fig. (8) for the Gaussian spectrum. Very good agreement is obtained apart from upstream angles. Similar results in terms of accuracy are obtained when considering either Liepmann or von Karman spectrum due to the fact that the turbulence spectrum only affects the absolute level of the directivity at a given frequency.

Results for evolving turbulence

In this section the generation of broadband noise due to the interaction of evolving turbulence with a flat plate is investigated. In contrast with the previous section, where results were ob-

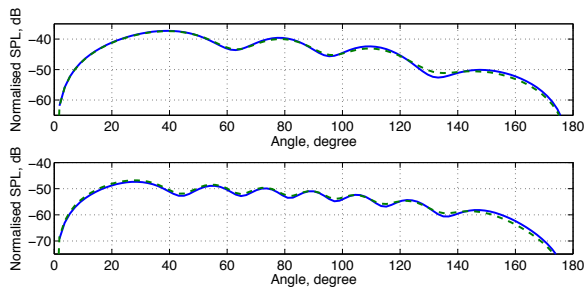


Figure 8: Analytical (—) versus numerical (---) far-field directivity using the Gaussian filter at $St = 2.03$ (top) and $St = 4.06$ (bottom).

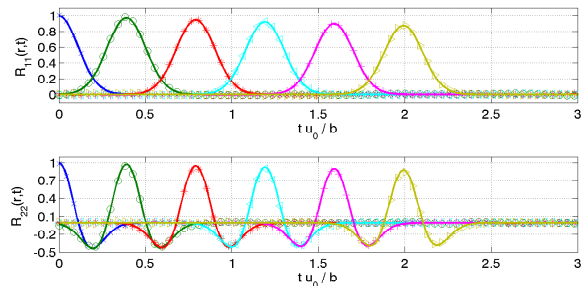


Figure 9: Two-point space-time analytical versus numerical R_{11} (top) and R_{22} (bottom) correlations. Solid lines stand for analytical results and symbols for numerical correlations obtained with the Langevin equation for points at distance: $r/b = 0$ (\times), $r/b = 0.4$ (o), $r/b = 0.8$ ($*$), $r/b = 1.2$ (\triangleleft), $r/b = 1.6$ ($+$), and $r/b = 2$ (\triangleright).

tained by assuming that the synthetic turbulent velocity field was a frozen pattern moving with the base flow, the effects of loss of correlation in time are now taken into consideration.

The validation of the evolving synthetic velocity field characterised by its integral time scale τ has been performed by computing two-point space-time correlations. Since the synthetic turbulent velocity field is used as a boundary condition in the linearised Euler equations along the flat plate, we are focussing on the two-point space-time correlation along the airfoil, $R_{ij}(r_1, t_1) = \langle u'_i(r_1, t_1) u'_j(r_2, t_2) \rangle$.

Fig. (9) shows numerical two-point space-time correlations for points along the airfoil at distances $r/b = 0, 0.4, 0.8, 1.2, 1.6$ and 2 from the leading edge against analytical results. Good level of agreement is obtained when comparing numerical and analytical R_{11} and R_{22} correlations for the different locations.

In contrast with the case of frozen turbulence, the maximum correlation decreases due to the influence of the temporal correlation of U modelled by the Langevin equation as $\exp(-t/\tau)$. Therefore, for this test case, the integral time scale of the turbulence τ provides about 12% loss of temporal correlation for points that are one flat plate apart.

The acoustic pressure field surrounding the flat plate generated by interaction with synthetic evolving turbulence is depicted in Fig. (10). In comparison with the acoustic pressure field generated by frozen turbulence, it shows a much larger content of noise with small wavelengths radiating from the airfoil, see Fig. (7). For the case with frozen turbulence, most of the noise is radiated from the leading edge and there is a secondary acoustic

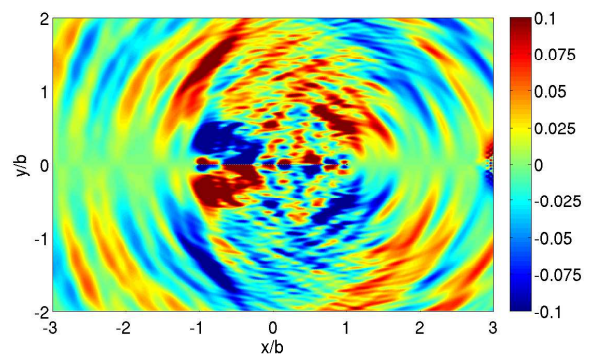


Figure 10: Snapshot of the acoustic pressure field for the Gaussian spectrum generated with a first-order Langevin model.

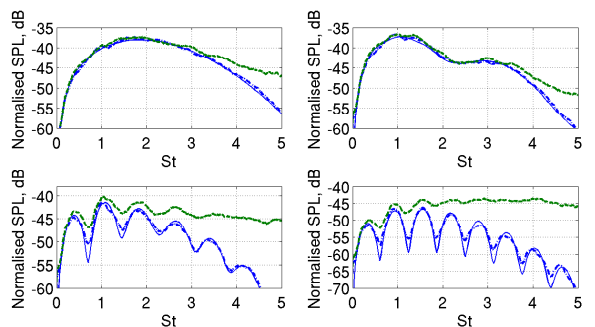


Figure 11: Normalised analytical (—) and numerical (---) SPL for frozen turbulence versus numerical (---) SPL for evolving turbulence. From top to bottom and left to right observers located at 30°, 60°, 120°, 150° of the airfoil.

scattering at the trailing edge. However, in this case, there are significant additional sources located mostly near the middle of the flat plate.

Fig. (11) shows the normalised sound pressure levels compared against numerical and analytical results obtained for the case of frozen turbulence ($\tau \rightarrow \infty$) for observers in the far field at 30, 60, 120, 150 degrees from the downstream direction. For observers located downstream, noise levels are similar to the case of frozen turbulence for Strouhal numbers smaller than 3 but there are much higher noise levels for higher frequencies. An even more significant increase between frozen and evolving turbulence is observed at upstream locations. Noise levels at 120 and 150 degrees are larger for evolving turbulence than those generated with frozen turbulence over the whole range of frequencies. In particular, at 150 degrees an almost flat spectrum is found for Strouhal numbers larger than 2. Even though the overall sound pressure levels in the upstream direction are about 10 decibels lower than the levels downstream, the large content of sound at high frequencies is significant.

At this point one might question whether the higher noise levels observed at high frequencies are a genuine effect of introducing time correlation in the synthetic velocity field or instead represent spurious sources introduced by the discretisation of the Langevin equation. A possible explanation could be a lack of numerical resolution in space or time, but this has been ruled out. The smallest hydrodynamic wavelengths are resolved by 17 points per wavelength and the smallest acoustic wavelengths by 35 points per wavelength in the frequency range of interest ($St = 0$ to 5). In addition, the solution seems also independent

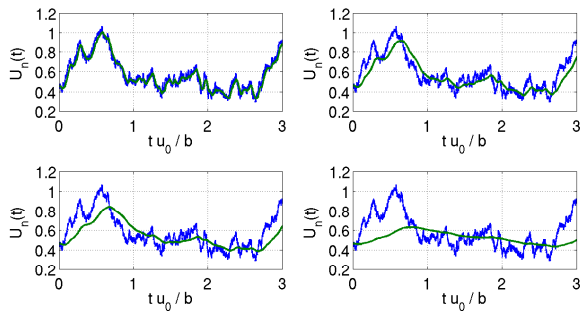


Figure 12: Time evolution of the strength of a given vortex-particle modelled by the Langevin equation (—) versus the strength modelled by the second-order Langevin model (---). Form top to bottom and left to right, $\tau_d = \tau/709$, $\tau_d = \tau/442$, $\tau_d = \tau/71$, and $\tau_d = \tau/18$.

of the time step used in the numerical integration. This suggests that the numerical results have fully converged.

The second-order Langevin model proposed in Eq. (23) requires the knowledge of the time scale τ_d which is used here as a numerical parameter to smooth the time evolution of the strength of the vortices.

In Fig. (12) the time evolution of a given vortex-particle modelled with the second-order Langevin model for different values τ_d are compared against the time evolution of the same vortex-particle modelled with the Langevin equation. We can see that a much smoother behaviour is obtained with the second-order model than with the Langevin equation. The largest the value of the τ_d is, the smoother the solution until the point where the strength is almost independent of time.

A parametric study was performed to select the value of τ_d . Its value must be sufficiently smaller than the integral time scale of the turbulence so that the resulting time correlation, Eq. (19) is a good approximation of $\exp(-t/\tau)$ and τ_d should be sufficiently large compared to the time step so that the solution converges at a reasonable computational cost.

From this parametric study we concluded that by selecting $\tau_d = \tau/71$ the statistical behaviour of the turbulence is accurately captured by the model and accurate far-field results can be obtained using the same time step as for the case of frozen turbulence.

Fig. (13) shows numerical two-point space-time correlations for points along the airfoil at distances $r/b = 0, 0.4, 0.8, 1.2, 1.6$ and 2 from the leading edge against analytical results. Good level of agreement is obtained when comparing numerical and analytical correlations R_{11} and R_{22} for the different locations.

A snapshot of the predicted acoustic pressure field around the flat plate is depicted in Fig. (14). Small acoustic wavelengths radiating from the middle of the flat plate predicted by the Langevin equation Eq. (14) are no longer present, see Fig. (10). In contrast, most of the noise is radiated from the leading edge as predicted by interaction with frozen turbulence, see Fig. (7).

Normalised sound power levels obtained by interaction with frozen turbulence and with evolving turbulence modelled by the second-order Langevin model are depicted in Fig. (15) for observers in the far field at 30, 60, 120, 150 degrees from the downstream direction. Numerical SPLs for evolving turbulence

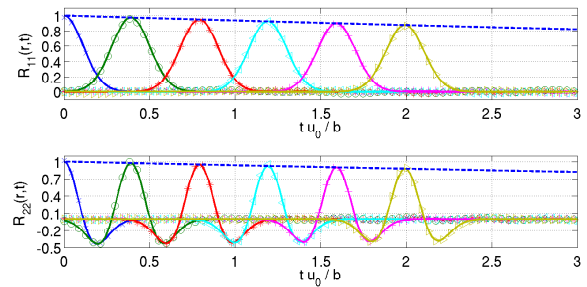


Figure 13: Two-point space-time analytical versus numerical R_{11} (top) and R_{22} (bottom) correlations. Solid lines stand for analytical results, dashed line is the temporal correlation $\exp(-t/\tau)$ and symbols for numerical correlations obtained with the Langevin equation for points at distance: $r/b = 0$ (\times), $r/b = 0.4$ (o), $r/b = 0.8$ ($*$), $r/b = 1.2$ ($<$), $r/b = 1.6$ ($+$), and $r/b = 2$ ($>$).

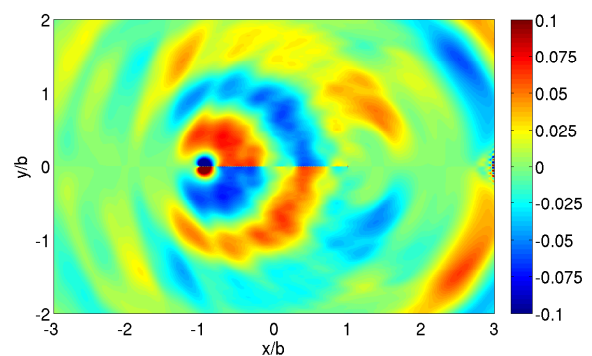


Figure 14: Snapshot of the acoustic pressure field for the Gaussian spectrum generated with a second-order Langevin model.

are depicted against numerical and analytical SPLs for the case of frozen turbulence. Similar results are obtained for the four locations either by assuming that the turbulence is frozen or by including the effects of time correlation through the second-order Langevin model. The only discrepancy found is at 150 degrees where when assuming evolving turbulence, sound power levels do not fully account for the interference pattern generated by interaction between the noise radiated from the leading edge and the scattering at the trailing edge.

Directivities at the Strouhal numbers $St = 2.03$ and $St = 4.06$ are shown in Fig. (16) where angles are measured from the downstream direction. Numerical results for evolving turbulence are depicted against numerical and analytical results for the case of frozen turbulence. Very good agreement is obtained for both Strouhal numbers between frozen and evolving turbulence apart from upstream directions where slightly different trends are found. This disparity for upstream directions can be related with the discrepancy found in the frequency spectra at upstream locations, see Fig. (15).

In summary, noise levels generated by interaction of evolving turbulence with the flat plate are similar to those obtained by interaction with frozen turbulence. Note that a characteristic time scale of a vortex passing through the leading edge is of the order of λ/u_0 which is more than a hundred times smaller than the integral time scale of the turbulence. Therefore, the strengths of the vortices vary very little as they pass near the leading edge generating almost the same velocity field as if their strength was kept frozen.

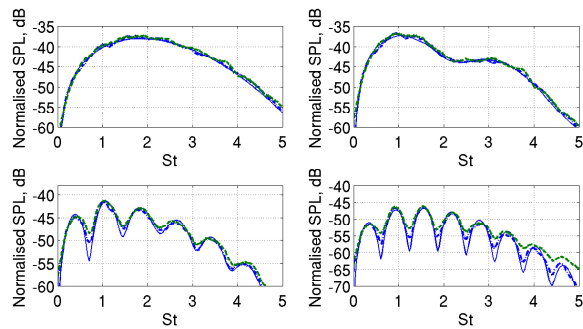


Figure 15: Normalised analytical (—) and numerical (---) SPL for frozen turbulence versus numerical (---) SPL for evolving turbulence. From top to bottom and left to right observers located at 30°, 60°, 120°, 150° of the airfoil.

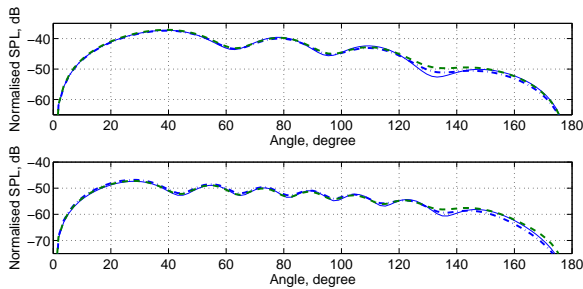


Figure 16: Far-field directivity at $St = 2.03$ (top) and $St = 4.06$ (bottom). Analytical (—) and numerical (---) directivity for frozen turbulence versus evolving turbulence (---) with $\tau_d = 0.2941$.

CONCLUSIONS

The random-vortex-particle model considered in this work is capable of efficiently reproducing the two-point space-time correlation tensor and a target value of the turbulent kinetic energy. It requires either an energy spectrum or a correlation function together with the kinetic energy and time and length scales. The energy spectrum can be chosen to provide the velocity field most suited for the specific problem under investigation. In this sense, three different energy spectra have been considered yielding different acoustic spectra and different computational costs.

Broadband fan interaction noise has been investigated by combining the linearised Euler equations with the method to generate synthetic turbulence. A general in-house finite-difference solver was used to implement the linearised Euler equations. The method was used to predict the broadband interaction noise generated by interaction between a two-dimensional flat plate and homogeneous isotropic turbulence.

The effects of generating the synthetic velocity field with the Gaussian, Liepmann or von Karman filters have been investigated for frozen turbulence. An extensive parametric study has been performed for each of the three filters under consideration in order to improve the accuracy of the synthetic turbulence method. This accuracy has been measured in terms of statistics along the flat plate and far-field spectra and directivities. Very good agreement between numerical and analytical correlations and one-dimensional energy spectra has been found. Regarding far-field results, the sound power levels seen by an observer at different locations around the airfoil are in good agreement

with the analytical proposed by Amiet that accounts for a fully two-dimensional problem. Directivities are also well predicted apart from upstream of the airfoil where the method is not able to fully capture the sound power levels. As it was expected, comparing far-field sound power levels at the same location but computed using different filters different amplitude of the noise levels at each frequency is found being the difference more noticeable at higher frequencies.

The effects of loss of correlation have been introduced in the random-vortex-particle method by modelling the rate of change in time of the strengths of the vortices through two Langevin models. The first of them is a Langevin equation with source term given by a white noise field. The statistical behaviour of the resulting evolving turbulence flow captures the loss of correlation in time and reproduces two-point space-time correlations along the flat plate accurately. However, it predicts spurious sources radiating from the flat plate. In order to remove these spurious sources a second Langevin model was proposed. In this case the forcing term is a continuous function correlated with the strength of the vortices so that the effects of viscous dissipation are included in the model. The resulting second-order Langevin model reproduces two-point space-time correlations along the flat plate and predicts far-field noise levels noise similar to those obtained by interaction with frozen turbulence. These results are supported by the fact that a characteristic time scale of a vortex passing through the leading edge is more than a hundred times smaller than the integral time scale of the turbulence. Therefore, the strengths of the vortices vary very little as they move past the leading edge and in consequence almost the same velocity field as if their strength was kept frozen is generated.

ACKNOWLEDGMENTS

This work is being supported by the Engineering and Physical Science Research Council (UK) and by Rolls-Royce plc through the Rolls-Royce University Technology Centre in Gas Turbine Noise at the University of Southampton.

REFERENCES

- [1] R. K. Amiet. Acoustic radiation from an airfoil in turbulent stream. *Journal of Sound and Vibration Research*, 4(4):407–420, 1975.
- [2] H. M. Atassi and M. M. Logue. Effect of turbulence structure on broadband fan noise. In *Proceedings of the 29th AIAA Aeroacoustics Conference*, Vancouver, Canada, May 2008. paper 2008–2842.
- [3] C. Bailly, P. Lafon, and S. M. Candel. Stochastic approach to compute subsonic noise using linearized euler’s equations. In *Proceedings of the 20th AIAA Aeroacoustics Conference*, Greater Seattle, Washington, May 1999. paper 1999–1872.
- [4] W. Bechara, C. Bailly, and P. Lafon. Stochastic approach to noise modelling for free turbulent flows. *AIAA Journal*, 32(3):455 – 463, March 1994.
- [5] M. Billson, L.-E. Eriksson, and L. Davidson. Jet noise prediction using stochastic turbulence modelling. In *Proceedings of the 24th AIAA Aeroacoustics Conference*, Hilton Head, South California, May 2003. paper 2003–3282.
- [6] A. Careta, F. Sagues, and J. Sancho. Stochastic generation of homogeneous isotropic turbulence with well-defined spectra. *Physical Review E*, 48(3):2279–2287, 1993.
- [7] D. R. Cox and H. D. Miller. *The Theory of Stochastic Processes*. Chapman and Hall Ltd, 1978.
- [8] M. Dieste and G. Gabard. Synthetic turbulence applied to

- broadband interaction noise. In *Proceedings of the 30th AIAA Aeroacoustics Conference*, Miami, Florida, May 2009. 2009–3267.
- [9] R. Ewert. Broadband slat noise prediction based on CAA and stochastic sound sources from a random-particle mesh (rpm) method. *Computers and Fluids*, 37:369–387, 2008.
- [10] R. Ewert and R. Emunds. CAA slat noise studies applying stochastic sound sources based on solenoidal digital filters. In *Proceedings of the 26th AIAA Aeroacoustics Conference*, Monterey, California, May 2005. paper 2005–2862.
- [11] R. Ewert, O. Kornow, B. J. Tester, C. J. Powles, J. W. Delfs, and M. Rose. Spectral broadening of jet engine turbine tones. In *Proceedings of the 29th AIAA Aeroacoustics Conference*, Vancouver, Canada, May 2008. paper 2008–2940.
- [12] M. Klein, A. Sadiki, and J. Janicka. A digital filter based generation of inflow data for spatially developing direct numerical or large eddy simulations. *Journal of computational Physics*, 186:152–665, 2003.
- [13] R. H. Kraichnan. Diffusion by a random velocity field. *The Physics of Fluids*, 13(1):22–31, 1970.
- [14] E. Krasnoff and R.L. Peskin. The langevin model for turbulent diffusion. *Geophysical Fluid Dynamics*, 2:123–146, 1971.
- [15] M. Omais and B. Caruelle. Jet noise prediction using rans cfd input. In *Proceedings of the 29th AIAA Aeroacoustics Conference*, Vancouver, Canada, May 2008. paper 2008–2938.
- [16] S. B. Pope. *Turbulent Flows*. Cambridge University Press, 2000.
- [17] M. Siefert and R. Ewert. Sweeping sound generation in jets realized with a random particle-mesh method. In *Proceedings of the 30th AIAA Aeroacoustics Conference*, Miami, USA, May 2009. paper 2009–3369.
- [18] A. A. Townsend. *The Structure of Turbulent Shear Flow*. Cambridge University Press, second edition, 1976.